Pulsed-laser-induced nanoscale island formation in thin metal-on-oxide films

S. J. Henley,* J. D. Carey, and S. R. P. Silva
Nano-Electronics Centre, Advanced Technology Institute, School of Electronics and Physical Sciences, University of Surrey, Guildford, GU2 7XH, United Kingdom

(Received 13 June 2005; revised manuscript received 21 September 2005; published 8 November 2005)

The mechanisms controlling the nanostructuring of thin metal-on-oxide films by nanosecond pulsed excimer lasers are investigated. When permitted by the interfacial energetics, the breakup of the metal film into nanoscale islands is observed. A range of metals (Au, Ag, Mo, Ni, Ti, and Zn) with differing physical and thermodynamic properties, and differing tendencies for oxide formation, are investigated. The nature of the interfacial metal-substrate interaction, the thermal conductivity of the substrate, and the initial thickness of the metal film are all shown to be of importance when discussing the mechanism for nanoscale island formation under high fluence irradiation. It is postulated that the resulting nanoparticle size distribution is influenced by the surface roughness of the initial film and the Rayleigh instability criterion. The results obtained are compared with simulations of the heat transfer through the film in order to further elucidate the mechanisms. The results are expected to be applicable to the laser induced melting of a large range of different materials, where poor wetting of substrate by the liquid phase is observed.

DOI: 10.1103/PhysRevB.72.195408 PACS number(s): 81.07.−b, 68.60.Dv, 78.70.−g

I. INTRODUCTION

Due to the short pulse duration and high power density of the excimer lasers, they can be used to rapidly introduce significant amounts of heat into a solid. The ablation, melting, and fast recrystallization produced by laser irradiation are processes which are widely exploited for a multitude of materials processing techniques. One such application is the crystallization of amorphous Si.[1] In addition, the effect of short pulse laser irradiation on metals is important for understanding material processing techniques such as laser machining and welding, and for obtaining high-temperature thermophysical data. The rapid heating and subsequent phase transitions that occur during short pulse irradaition can be complex, and have been the subject of theoretical and experimental investigations.[2–5] However, the majority of these studies of laser irradiation of materials concentrate on the surface melting and ablation of *thick* films and do not consider the effect of the material-substrate interaction.

Once a thin film is molten, instability driven breakup into droplets may be expected if the liquid phase poorly wets the substrate. This is similar to the island formation observed during the thermal annealing of thin metal films, such as Ni. Here a weak interaction between the metal and the oxide layer results in a low activation energy barrier for metal migration, even at temperatures well below the melting point of the metal.[6,7] In thin film deposition the growth of nanostructured surfaces depends on the growth mode. Layer-by-layer or two-dimensional (2D) growth is called the Frank–Van der Merwe mode,[8] 3D island growth occurs in the so-called Volmer-Weber mode,[7,9] and initial 2D growth of a few monolayers thick wetting layer, followed by 3D growth, is referred to as the Stranski-Krastanow mode.[10] The growth mode that occurs is influenced by the relative weight of the free enthalpy of the substrate surface, that of the surface of the film, and of the interface between the film and the substrate. Similarly, during the thermal annealing of thin films, the morphological stability and fragmentation dynamics are also controlled by the free enthalpy. For very thin metal films on oxide surfaces, where the metal does not react readily with the oxide, this break up during thermal annealing allows the self-assembly of supported nanoparticle arrays.[6,11] Here, the enthalpy of formation of the metal oxide is a critical parameter determining the relaxation dynamics, but are similar effects expected during the short pulse laser melting of *thin* metal-on-oxide films?

Nanoparticle systems currently attract considerable interest from both academia and industry, due to their interesting and diverse properties, which deviate from those of the bulk. Metal nanoparticles and other metal nanostructures are the basic building blocks in photonics research[12] and it is expected that magnetic nanoparticles will have a dramatic impact on high density magnetic recording[13] and radar-absorbing composite applications.[14] Transition metal nanoparticles, such as Ni, Co, Fe, and Au are of considerable importance for the catalytic growth of nanostructures including carbon nanotubes[11,15,16] and silicon nanowires.[17] Nanoparticle systems are also of significant interest to the fuel cell community, working to increase the reaction surface for a fixed cell volume. Nanoparticle systems can be fabricated by a large range of different techniques including chemical reduction,[18] laser ablation,[19] thermal evaporation,[20] ion implantation,[21] and thermal annealing.[6,11]

In this paper we investigate the physical mechanisms behind the pulsed laser melting of thin metal-on-oxide film and use this technique, entitled excimer laser nanostructuring (ELN), to produce supported metal nanoparticles, with controllable dimensions, over large area and at low macroscopic temperatures. Previously, we demonstrated that ELN of thin Ni films can be used to produce nanoscopic Ni catalyst particles suitable for the growth of carbon nanotubes.[16] Here we examine the underlying mechanisms of the ELN technique more closely, for a carefully chosen selection of metals with differing physical and thermodynamic properties, and differing enthalpies of formation for the oxide. We discuss how this process differs from the traditional thermal annealing

method of producing nanostructured metal-on-oxide substrates and compare the experimental data obtained during ELN of thin metal films with simulations of the heat transfer.

II. EXPERIMENTAL DETAILS

The ELN of a variety of metal thin films on SiO_2/Si substrates was investigated in order to determine what materials and laser parameters are required to produce metal nanoparticles. The initial thin films were produced by pulsed laser ablation[22,23] (PLA) of a high purity metal targets (all materials had a purity >99.9%). A Lambda-Physik LPX 210i excimer laser, producing 25 ns pulses at 248 nm, was used for the ablation. The growth chamber was evacuated using a turbo pump to 9×10^{-8} Torr and the typical laser fluence used was 10 J/cm^2. The metals investigated here were Au, Ag, Ni, Mo, Ti, and Zn. The growth rate for each metal was calibrated by measuring the thickness of a range of films, deposited with different numbers of laser shots, by a combination of atomic force microscopy (AFM) and profilometry.

Some of the films have a low density of hydrodynamically "splashed" micron-sized droplets, which are typical for pulsed laser deposited films,[22] but in general the films were very smooth. The PLA technique has been used to deposit very smooth films for a wide variety of metals. For very thin films (<5 nm) island growth is observed in some systems, however in general at high fluences like those used here, the high flux of energetic (hundreds of electron volts) metal atoms and ions produces smooth films and in some cases epitaxial growth.[24] By reducing the kinetic energy of the growth species, e.g., by introducing He during the growth,[25] nanostructured films can be deposited directly for some metals. However, above a few nanometers thick, these films consist of conglomerated, rather than isolated, nanoparticles. The surface roughness of a selection of the films was examined in the AFM and was typically <1 nm. Thin films with thickness in the range 5–20 nm were then deposited onto a SiO_2 layer of 235 nm thickness, thermally grown on a Si substrate, for subsequent laser processing.

The thin films were ELN using the same excimer laser as employed for the deposition, by diverting the optical path and passing it through a homogenizer, producing a laser spot with a Gaussian energy profile along one axis, the peak fluence of the profile being ~ 1.5 times the average. The films were transferred to a separate vacuum stage (typical working pressure 10^{-4} Torr) where the whole sample could be annealed by translating the stage. Typical translation rate was 1 mm/s with a laser repetition rate of 10 Hz. The number of laser pulses any area receives is ~50 but due to the Gaussian beam profile, only the area at the central part of the beam receives the full laser energy. Post-annealing the structure of the films was investigated in a Hitachi S4000 field emission gun scanning electron microscope (SEM) with a spatial resolution of 1.5 nm. The size distribution of any metal nanoparticles produced was obtained using commercial image analysis software.[26]

III. RESULTS AND DISCUSSION

A. Effect of film thickness and laser fluence

The Ni on SiO_2 system is typically classified as a relatively unreactive pair,[27,28] as Ni, compared to more reactive metals, does not readily form an oxide (the heat of formation of the oxide is −241 kJ mol^{-1}). The melting point of Ni, of 1728 K, is also intermediate between the very high and very low melting point metals. Thus this system is an ideal starting point to investigate the laser induced nanostructuring of thin metal films. Figures 1(a)–1(d) show a series of SEM images of a selection of the laser annealed films, with different initial Ni thickness, grown on 320 nm SiO_2/Si substrates.[16] The ELN was performed at laser fluences of ~200 mJ/cm^2. After exposure to the laser the Ni film was observed to have melted and then broken up into discrete nanometer-scale hemispherical islands. The fluence required to achieve this breakup was a function of the initial film thickness and the thickness of the oxide layer on the substrate. Higher laser fluences were required to nanostructure the thinner Ni films. This indicates that we are in a region where the heat conduction out of the film into the substrate is significant. At lower fluences the films were observed to perforate, but the breakup into discrete droplets was incomplete. These measurements were repeated for Ni films deposited onto Si substrates with a thinner oxide later. The fluences required to nanostructure the films grown on the thinner 235 nm thermal SiO_2 substrates were higher than for the corresponding Ni film on the thicker 320 nm SiO_2 layers. This confirms the importance of heat conduction during the duration of the laser pulse. At fluences higher than the threshold for breakup, no change in the Ni droplet size distribution was observed; the defining parameter which determines the droplet size was the film thickness. However, the maximum fluence achievable by the optical system was 700 mJ/cm^2, so we could only investigate the effect of laser fluence up to this value. Figure 1(e) shows a plot of the mean particle diameter for the ELN of Ni films as a function of initial film thickness. The mean particle diameter is observed to increase as the initial film thickness increases. The relationship between the diameter and the film thickness will be discussed in more detail later.

In order to investigate the general properties of the ELN of thin metal films, the measurements were repeated for a range of different metals including Au, Ag, Mo, Zn, and Ti. This range of materials were chosen as they have properties which span a wide range of values and span different classes of metals. For example, Zn and Mo have melting points that differ by a large amount (693 K for Zn compared to 2905 K for Mo). Also, Au and Ti are examples of metals that hardly oxidize and readily form an oxide, respectively, so should give us a good insight into the effects of the metal-substrate interaction on the ELN. Films with a thickness of 5, 10, 15, and 20 nm were deposited for all these metals, on 235 nm SiO_2/Si substrates, and were subsequently laser irradiated at fluences in the range 75–700 mJ/cm^2. Figure 2 shows SEM images of ELN Mo films (a) before, (b) close to, and (c) after the threshold fluence for nanostructuring. Note the initial film in (a) and (c) was 20 nm thick and in (b) 15 nm thick. The laser fluence was around 660 mJ/cm^2 in all cases. Just below the break-up threshold the films perforate and the molten film around these perforations is observed to have drawn away from the center of the hole [as is shown in Fig. 2(a)]. These perforations are likely to occur at thickness inhomogeneities in the film, as the fluence required for melting is

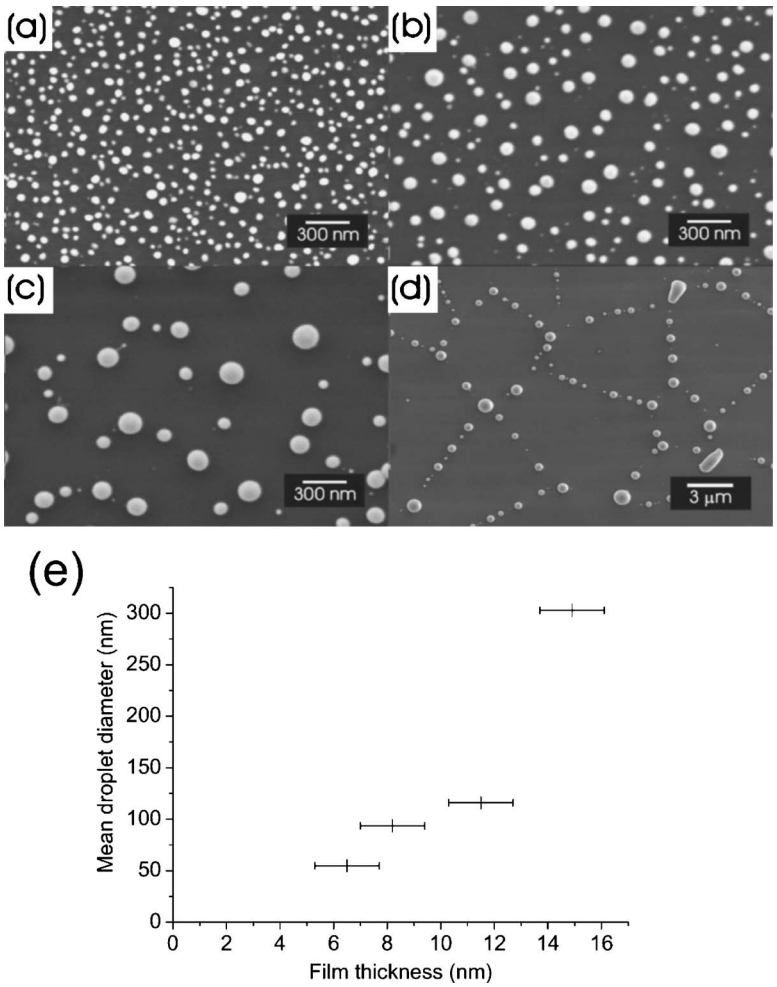

FIG. 1. (a)–(d) SEM images of ELN Ni films with different thicknesses. (a) 6.5 nm thick film, (b) 8.2 nm, (c) 11.5 nm, and (d) 15 nm. Note the different scale bar on image (d). (e) Plot of the mean particle diameter for the ELN of Ni films as a function of initial film thickness.

predicted to be lower for thicker films. This will be discussed in more detail later. When the density of perforations is high, the retreating molten film between two holes can coalesce into filaments, as is shown in Fig. 2(b). At fluences slightly higher than the threshold these filaments, or liquid metal nanowires, can then split into droplets possibly due to the Rayleigh instability[29] which has been recently observed experimentally for thermally annealed Cu nanowires on SiO_2 surfaces.[30] A clear example of these chains of droplets can be seen for Ni in Fig. 1(d). The fluence required to melt the Mo films is much higher than that for the same thickness of Ni, mainly a consequence of its higher melting point (1718 K for Ni compared to 2905 K for Mo).[31] The propensities for oxide formation are similar for the two metals, thus the comparison investigates the effects of the differing thermal properties of the metals, rather than the metal-substrate interaction.

In order to investigate the effects of ELN at fluences much greater than the break-up threshold it was decided next to look at thin Au and Ag films, which have lower melting points than Ni or Mo. Figure 3 shows two sequences of SEM images of the ELN of (a)–(d) and 15 nm thick Ag (e)–(h) films. The fluences used on the Au films were (a) 0 mJ/cm^2, i.e., unannealed to show that the film is continuous and smooth on this scale, (b) 125 mJ/cm^2, (c) 250 mJ/cm^2, (d) 430 mJ/cm^2, and for Ag (e) 0 mJ/cm^2, (f) 150 mJ/cm^2, (g) 300 mJ/cm^2, and (h) 400 mJ/cm^2. The initial sequence of perforation and breakup into droplets was similar for Au and Ag as was observed for Ni and Mo. However, well above the threshold [see Figs. 3(c) and 3(g)] smaller droplets are observed around the larger ones. At the highest fluences studied [see Figs. 3(d) and 3(h)] all the large droplets are gone and are replaced by a high density of much smaller droplets. Statistical analysis of the Ag nanoparticle diameter distributions produced by the ELN of a 5 nm Ag thin films at fluences of (a) 175 mJ/cm^2, (b) 250 mJ/cm^2,(c) 400 mJ/cm^2, and (d) 600 mJ/cm^2 are shown in Fig. 4. From these distributions we can observe a shift of the distribution from a mean diameter of 43 nm down to 17 nm, as the fluence is increased. The larger diameter droplets fragment into smaller droplets, at higher temperatures, possibly as they boil. By examining the size distribution for the larger droplets, produced at lower fluences, as a function of film thickness (not shown here) it is seen that the mean size is again dependent on the initial film thickness. However, the mean size of the droplets produced at high fluence is relatively insensitive to the film thickness. It appears that, at the higher relative fluences, it is possible to start to evaporate the droplets and at the highest fluences, to fully ablate away the film, leaving a distribution of nanoparticles only formed as the last of the film boils away. Indeed, at the highest fluences used, a thin coating was observed on the glass of the laser annealing chamber opposite the films, indicating that the material had been ablated.

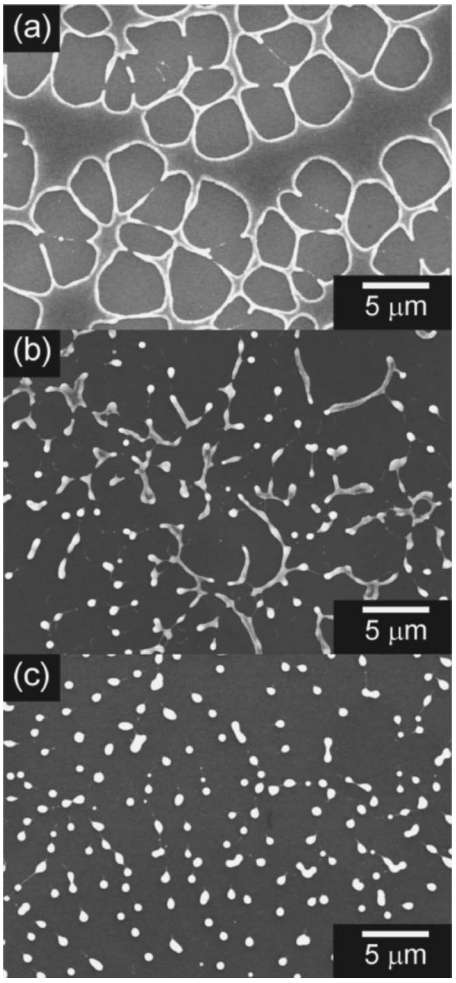

FIG. 2. SEM images of ELN Mo films (a) before, (b) close to, and (c) after the threshold fluence for nanostructuring. Note the initial film in (a) and (c) was 20 nm thick and in (b) 15 nm thick.

B. Effect of metal-substrate interaction

Very similar behavior was observed for the four different metals discussed until now. It is thus feasible to question if this is a general property for the metal/SiO_2 system. Figure 5 shows SEM images of the metal droplets produced by the ELN of (a) a 20 nm Au film, (b) a 0 nm Ag film, (c) a 15 nm Ni film, and (d) a 20 nm Mo film. The samples have been tilted to show the droplets side on. The poor wetting of the SiO_2 by the liquid noble metal droplets is evidenced by the large contact angle between the droplet and the substrate. For Ni and Mo, the wetting is improved and the contact angle is reduced. Experimental contact angles for metal droplets on ionocovalent oxide substrates have been obtained from sessile drop measurements.[27] From these measurements the contact angles for the Ag/SiO_2 and Ni/SiO_2 systems are given as $\sim 140°$ and $\sim 120°$, respectively. For the droplets produced in this study the contact angles are estimated from a series of images similar to those shown in Fig. 5. The values obtained were $\sim 120°$ for Au, 118° for Ag, 105° for Ni, and 72° for Mo. In the case of Ti/MgO however, formation of Ti oxide at the interface is expected[27] and the metal-oxide pair is classified as reactive, where the resultant contact angle is 0° and the metal wets the oxide. Figure 6 shows a SEM image of a 20 nm thick Ti film (a) before and (b) after laser irradiation at 250 mJ/cm^2. Although melting and roughening of the surface is clearly evident after irradiation, no droplet production is observed even at the highest fluences available. The melting point and thermodynamic properties of Ti are more favorable for melting than those of Mo (for example, the melting point is 1941 K and its thermal conductivity is only 0.22 $W\,cm^{-1}\,K^{-1}$), but no breakup into nanodroplets is observed. Similar behavior is observed for the Zn/SiO_2 system. The melting point of Zn is very low (693 K) but still no droplet formation is observed. This suggests that the interfacial metal-substrate interaction is critical for nanoparticle production by this method. To examine this more carefully we can compare the enthalpy of formation of the oxides $-\Delta H_f$ for the metals in question. These data, and the values for a selection of other elements are shown in Table I. Of the metals studied here, the ones that break up into droplets (Au, Ag, Ni, and Mo) are all in the top half of Table I, with $-\Delta H_f < 300$ kJ mol^{-1}. Those that wet the substrate (Zn and Ti) have $-\Delta H_f > 300$ kJ mol^{-1}. From Fig. 5, the observed contact angles between the metal drops and the SiO_2 substrate are observed to decrease as the value of $-\Delta H_f$ for the metal increases. For example Au, which does not readily form an oxide, produces near spherical droplets whereas Mo, which has a larger heat of formation, produces droplets with a contact angle less than 90°. Of course, ΔH_f is not the only parameter affecting the wetting, and we should also consider others including the work of adhesion.[27] However, it appears for this application that ΔH_f is a critical parameter and the breakup into droplets is controlled by the metal-substrate interaction.

C. Simulation

Before the breakup into droplets is possible, the film must first be brought to its melting point. It is important therefore, to consider the heat transfer that occurs during the pulsed laser melting of thin films. When laser photons are incident on a solid, the energy is typically absorbed by electronic excitations. These excitations rapidly decay and the energy is converted to heat over a time scale of the order of a few picoseconds.[32] The rapid heating and subsequent phase transitions can be complex, and have been the subject of theoretical and experimental investigations.[2,4,5] With the pulse duration of the excimer lasers typically being a few tens of nanoseconds, we can describe the temperature changes that occur in the solid using the heat conduction equation, by introducing a source term. As the power density is uniform over the irradiated area, which is large compared to the film thickness, the heat conduction can be considered only in one spatial dimension. Hence, the heat conduction equation takes the form

$$c\rho\frac{\partial T}{\partial t} = I(z,t)\alpha + \frac{\partial}{\partial z}\left(\kappa\frac{\partial T}{\partial z}\right), \tag{1}$$

where c is the heat capacity, ρ is the mass density, $T(z,t)$ is the temperature at depth z and time t, I is the laser power density, α is the absorption coefficient, and κ is the thermal

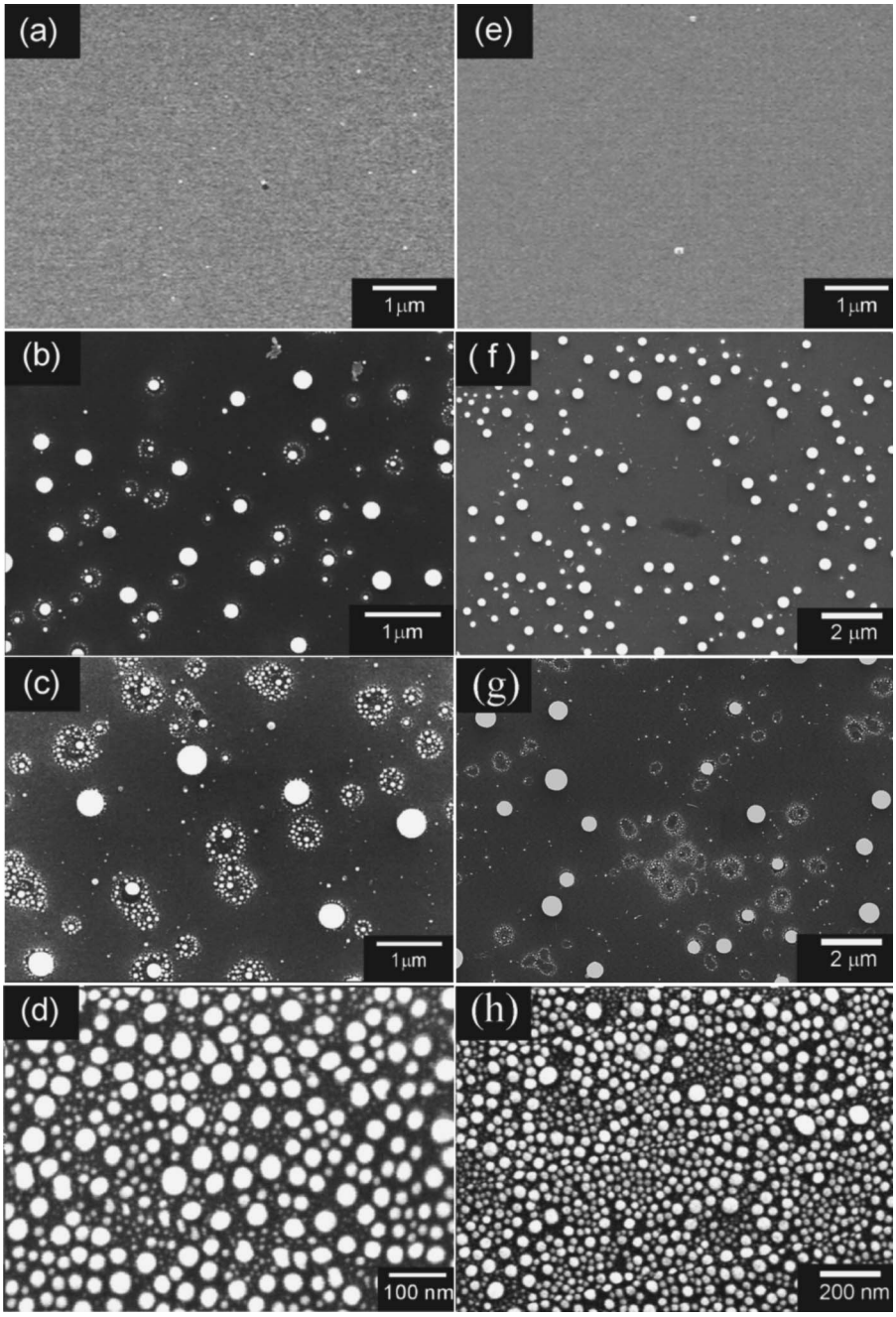

FIG. 3. SEM images of ELN 20 nm thick Au (a)–(d) and 15 nm thick Ag (e)–(h) films. The fluences used on the Au films were (a) 0 mJ/cm^2, i.e., unannealed, (b) 125 mJ/cm^2, (c) 250 mJ/cm^2, (d) 430 mJ/cm^2, and for Ag (e) 0 mJ/cm^2, (f) 150 mJ/cm^2, (g) 300 mJ/cm^2, and (h) 400 mJ/cm^2.

conductivity. z is taken to be zero at the surface of the metal film.

Before describing methods for solving this equation, a simple model to examine the general properties of the melting of thin film by pulsed lasers is proposed. The total heat Q, per unit area, deposited in a thin film modeled as a single layer of thickness d, irradiated by a single laser pulse of duration Δt with a top-hat temporal profile is given by Eq. (2).

$$Q = I\Delta t(1-R)[1-\exp(-\alpha d)], \tag{2}$$

where R is the reflectivity of the film material at the laser wavelength. Here we should consider the effect of interference due to reflections at the interfaces. We suggest that this will not be a very significant effect as the reflection coefficient at the metal-SiO_2 interface will be low (similar real parts of the refractive index and high transmittance in the UV for the SiO_2.) The laser energy that then reflects off the SiO_2-Si interface and then is not reflected again at the SiO_2-metal interface (high reflectivity is expected here due to the large imaginary part of the metal's refractive index) should only be a small contribution to the heating in the film. As the temperature rise in a thin film of thickness d, supplied with energy Q (ignoring heat conduction for now) is $\propto Q/d$, we see that in the limit of small d we get

$$\lim_{d\to 0}\frac{1-\exp(-\alpha d)}{d} = \alpha. \tag{3}$$

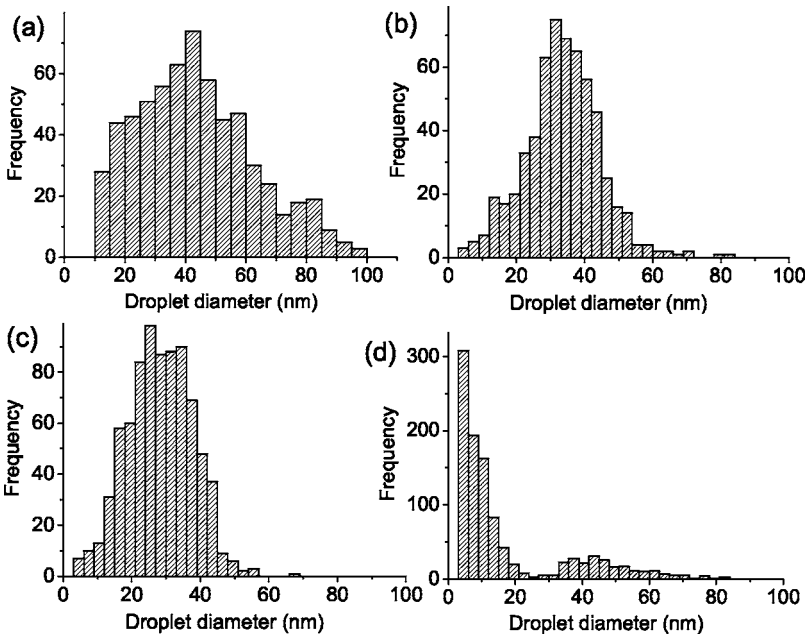

FIG. 4. Histograms of the Ag nanoparticle diameter distributions produced by the ELN of 5 nm Ag thin films at fluences of (a) 175 mJ/cm^2, (b) 250 mJ/cm^2, (c) 400 mJ/cm^2, and (d) 600 mJ/cm^2.

Thus, the temperature rise for very thin films, ignoring heat conduction, is expected to be significant if α is large, and thicker films should require higher laser fluences to melt. However, by observing the terms of Eq. (1), we can see that the rate of heat diffusion, into the substrate, for a thin film heated from the top surface will become greater as the film thickness decreases due to the temperature gradient across the film increasing. When heat conduction is considered, for thin films where $d<1/\alpha$, a region of the substrate determined by the thermal diffusion depth of SiO_2 will also be heated. The heat Q absorbed in the metal will also have to heat this region. Thus, the fluence required to melt the film will increase with decreasing d. For thicker films ($d>1/\alpha$), heat conduction into the substrate will be significantly slower and lower melting fluences would be expected. When $d \gg 1/\alpha$ partial melting of the top surface of the film should occur.

In order to model the system, Eq. (1) can be solved analytically under the assumption of no phase change occurring and that the thermal properties of the film remain constant. However, the thermal conductivity and heat capacity are both temperature dependent and we are considering a phase change from solid to liquid. Thus, Eq. (1) can only be solved numerically. Here we introduce a finite element model, where the film is split into layers of thickness Δz and the time proceeds in steps of Δt. The same method has been used to model the pulsed laser annealing of a variety of materials including amorphous silicon.[4] The energy absorbed by the ith layer, at depth z_i into the film, over the interval Δt is then

$$\Delta Q_i^a = I(z_i,t)[1-\exp(-\alpha\Delta z)]\Delta t, \tag{4}$$

where the laser power density $I(z_i,t)$ is given by

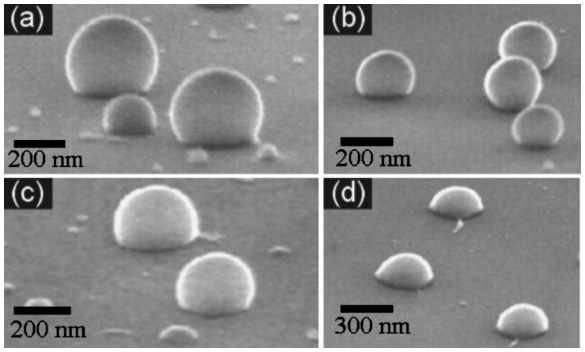

FIG. 5. SEM images of the metal droplets produced by the ELN of (a) a 20 nm Au film, (b) a 20 nm Ag film, (c) a 15 nm Ni film and (d) a 20 nm Mo film. The samples have been tilted to show the droplets side on.

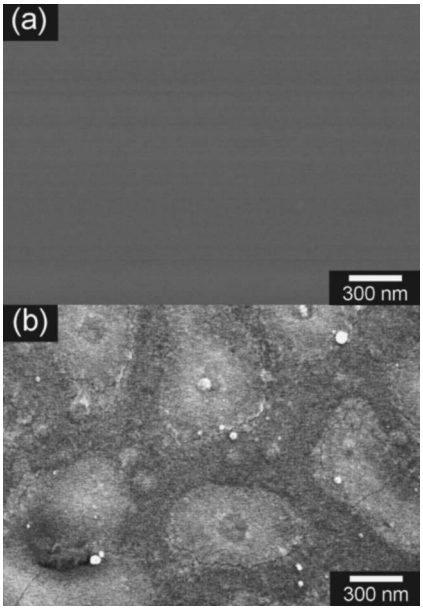

FIG. 6. SEM image of a 20 nm thick Ti film (a) before and (b) after laser irradiation at 250 mJ/cm^2. Although melting and roughening of the surface is clearly evident, no droplet production is observed even at the highest fluences available.

TABLE I. Enthalpy of formation $-\Delta H_f$ of the oxide per mole of O for a selection of metallic elements (Ref. 35).

$-\Delta H_f$(kJ mol^{-1})	Element
<0-50	Au, Ag, Pt
50–100	Pd, Rh
100–150	
150–200	Ru, Cu
200-250	Re, Co, Ni
250–300	Na, Fe, Mo, Sn, Ge, W
300–350	Rb, Ce, Zn
350–400	K, Cr, Nb, Mn
400–450	V
450–500	Si
500–550	Ti, U, Ba, Zr
550–600	Al, Sr, La, Ce
600–650	Mg, Th, Ca, Sc

$$I(z_i,t) = (1-R)I_0(t)\exp(-\alpha z_i). \tag{5}$$

The heat that diffuses into layer i Q_i^{diff} is determined by the temperature of the surrounding layers and is given by

$$\Delta Q_i^{\text{diff}} = \left(\kappa_a \frac{T_{i-1}-T_i}{\Delta z} + \kappa_b \frac{T_{i+1}-T_i}{\Delta z}\right)\Delta t, \tag{6}$$

where κ_a and κ_b are the average of the temperature dependent thermal conductivities at the "slice $i-1$/slice i" interface and the "slice i/slice $i+1$" interface, respectively. The temperature rise of slice i is thus

$$\Delta T_i = \frac{\Delta Q_i^a + \Delta Q_i^{\text{diff}}}{c(T_i)\rho\Delta z}, \tag{7}$$

where $c(T_i)$ is the temperature dependent thermal capacity. When a slice reaches its melting point, no temperature rise is allowed until the layer has absorbed enough energy to supply the required latent heat of fusion. The data used for the simulation is shown in Table II. The choice of Δz is crucial for this method to converge to the solution of Eq. (1). If $\Delta z \gg 1/\alpha$, then the simulation averages out the temperature rise that would have occurred at finer resolutions near the surface of the film. If Δz is too small then the temperature differentials between adjacent layers can be too large for the simulation to converge to the solution. For every order of magnitude finer spatial resolution, we require a two orders of magnitude finer temporal resolution to compensate. For the simulations presented later, the typical slice thickness Δz used was $\sim 1/2\alpha$ for the material in question. Thus, only a few layers were used in each simulation. The high thermal conductivity of the metal means that the film is essentially all at the same temperature throughout its depth and the temperature gradient is only large at the interface. The number of layers used for the metal does not have to be large to adequately model the system. Here we have used more layers for the substrate, where the temperature gradient is generally larger. The substrate was modeled as 12 SiO_2 layers (with a total thickness of 240 nm to match with the oxide thickness used in the experiments) with its own temperature dependent thermal properties. However, the bottom layer had its temperature fixed at room temperature and hence acts as a heat sink rendering the substrate effectively infinite in extent.

Now that a reasonable idea of the critical parameters has been obtained, our goal is to develop a predictive model that could be employed to estimate the threshold fluence for systems where the interfacial film-substrate interaction promotes nanoparticle production. Here, we apply the finite element model [see Eqs. (4)–(7)] in an attempt to simulate the melting of thin Ni, Au, Ag, and Mo films on SiO_2. We will then compare the predicted threshold melting fluences, as a function of d, with those observed experimentally, which are shown in Fig. 7 for Ag, Au, Mo, and Ni films.

Figure 8(a) shows a simulated temperature temporal profile for the surface layer of a 20 nm Ni thin film irradiated at a fluence equivalent to an experimental exposure of 330 mJ/cm^2. Four Ni layers were used for the simulation. The surface temperature is seen to rise rapidly at the start of the pulse, to level out as the film melts, then to increase again. After the laser pulse ends the film rapidly cools to near room temperature in $\sim$100 ns. It is observed immediately that this simulation predicts that rapid cooling through heat conduction into the substrate severely limits the maximum temperature obtainable at a given fluence. As expected, the cooling rate is sufficiently high so that each laser shot can be

TABLE II. Physical (Ref. 31), thermal (Ref. 31), and optical (Ref. 34) properties used for ELN simulations.

	Ni	Au	Ag	Ti	Zn	Mo	SiO_2
Melting point T_m (K)	1728	1337	1235	1941	693	2905	1983
Boiling point (K)	3186	3129	2435	3560	1180	4912	
Density (g/cm^3)	8.9	19.3	10.5	4.51	7.14	10.2	2.53
Heat capacity [J/(gK) at 25 °C]	0.444	0.129	0.235	0.523	0.388	0.251	0.73
Thermal conductivity [W/(cmK) at 25 °C]	0.907	3.17	4.29	0.219	1.16	1.38	0.014
Latent heat fusion (J/g)	305.6	222.1	200.8	332.3	130.6	639.7	
Reflectivity (% at 248 nm)	45.0	32.9	26.9			69.5	
Absorption coeff. (cm^{-1} at 248 nm)	1063830	829187	683995			1834862	
Surface tension at T_m (dyne/cm)	1778	1140	903	1650	782	2250	

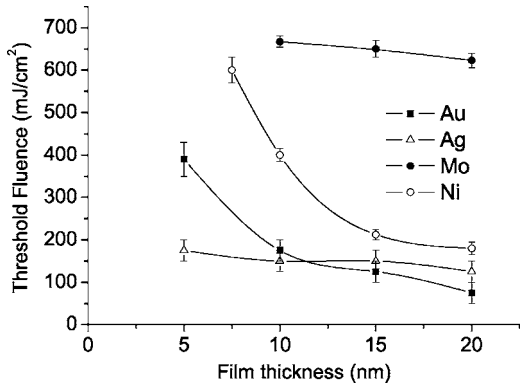

FIG. 7. Plot of the experimentally observed melting fluence of Ag, Au, Mo, and Ni thin films as a function of the film thickness. The lines are merely guides for the eye.

treated independently as the time between laser shots is around 0.1 s compared to the cooling time which is of the order of 10^{-7} s. Figure 8(b) shows a plot of the simulated fluence required to melt Ni, Au, and Ag films of different thickness. It was not possible to simulate the melting of the Mo thin films accurately as the melting point of Mo was higher than the melting point of SiO_2 and the finite element method used could not contend with the large temperature gradients that resulted. The predicted fluences are observed to compare favorably with the measured values. The predicted threshold fluences for Ni are closer to the measured

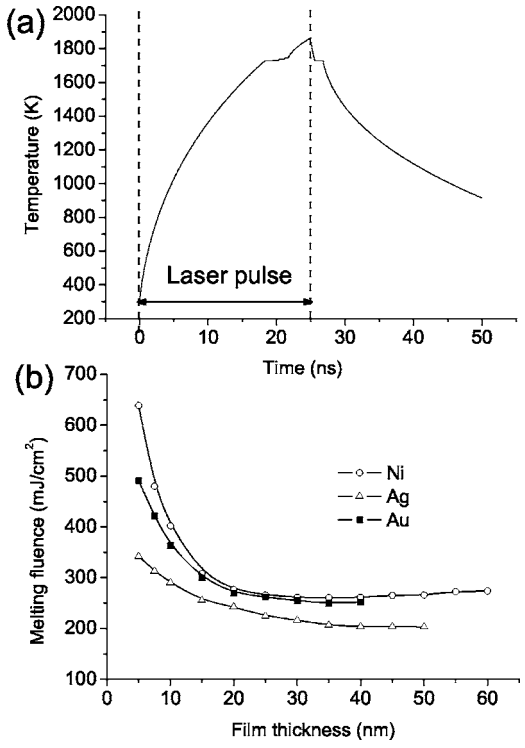

FIG. 8. (a) Simulated temperature temporal profile for the surface layer of a 20 nm Ni thin film irradiated at a fluence equivalent to an experimental exposure of 330 mJ/cm^2. (b) Plot of the simulated fluence required to melt Ni, Au, and Ag films of different thickness.

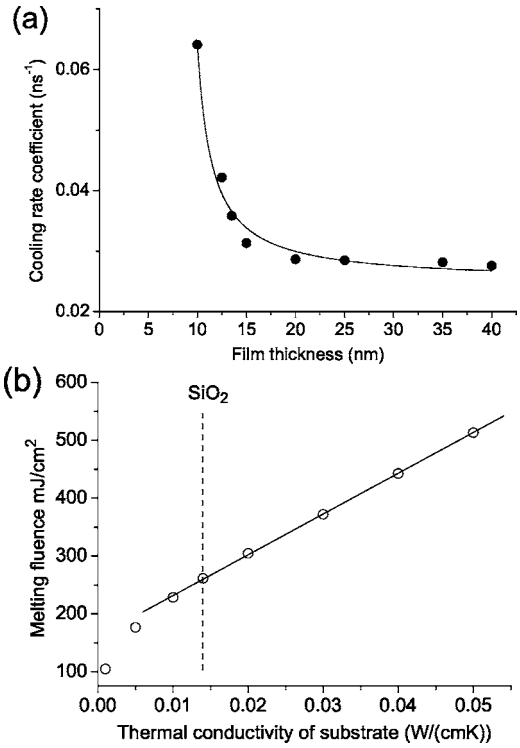

FIG. 9. (a) Calculated cooling rate coefficient (assuming an exponential decay) for the cooling of the surface layer of Ni thin films of different thickness, initially at T_m. (b) Plot of the calculated melting fluence for a 30 nm thick Ni thin film as a function of the room temperature thermal conductivity of the substrate.

values, than those of Ag and Au but the simulation appears to overestimate the fluence required to melt the thin Au and Ag films. In addition, the general form of the dependence of threshold with thickness is close to that observed. It is suggested that the threshold discrepancy can be attributed to the uncertainty of the parameters used. In all cases the values are for high quality bulk materials, but here it is expected that we are investigating defective or amorphous nanoscale films. Indeed, the melting points of films with nanometric thickness have been shown to be lower than that of bulk material.[33]

As we observed in this study and previously,[16] the thermal conductivity of the substrate and the initial film thickness were both critical parameters in determining the threshold fluence for nanostructuring Ni thin films. Using the present simulation, we can investigate this directly by varying the thermal conductivity of the substrate and the film thickness and observing the change in the melting fluence and the cooling rate. Figure 9(a) shows the calculated cooling rate coefficient k (assuming an exponential decay of the temperature, with time t, of the form $\exp^{-kt}$) for the cooling of the surface layer of Ni thin films of different thickness, initially at T_m, on SiO_2. The cooling rate is observed to increase significantly as the film thickness d decreases. Figure 9(b) shows a plot of the calculated melting fluence for a 30 nm thick Ni thin film as a function of the room temperature thermal conductivity κ_s of the substrate. Here the threshold fluence is observed to vary linearly with κ_s, apart from at very small values of κ_s. By comparing the results of the simulation and the experiments with the simple model pro-

posed by Eq. (3), it can be seen that the heat conduction out of thin films is a very important consideration for this system as the threshold fluence increases rapidly as d decreases rather than converging to a constant value.

D. Nanostructuring mechanisms

Based on the validated simulation of the melting of very thin metal films by pulsed laser irradiation developed in this study, we can now suggest a set of mechanisms for the ELN for the production of metal nanoparticles. At the onset of laser irradiation, the film temperature rapidly rises during the pulse. The rate of temperature rise is determined by the rate of heat conduction out of the film. If the film gets hot enough to melt, and the liquid phase poorly wets the substrate, breakup into droplets is likely. The question then arises: Is the breakup a self-ordering phenomenon, or can some parameter of the film account for the droplet size observed? At thickness inhomogeneities in the film, the fluence required for melting will change. For thick films the root mean square surface roughness is expected to be lower than that for the thinner films. However, even if the roughness remains unchanged, a 1 nm fluctuation will produce a much more significant local change in threshold fluence for a 5 nm thick film than for one 15 nm thick. We can observe this directly if we consider the derivative of the curves in Fig. 8(b), which is lowest at the largest thickness. Thus, we expect local hot spots (at thicker areas) to be a much rarer phenomenon for thick films than for thinner ones. In the regime where volume is conserved (no ablation), the nanoparticle radius R would be expected to be determined by Eq. (8)

$$\text{Volume of droplet } V_d = \frac{4\pi R^3}{3} \propto \frac{L^2 d}{N}, \tag{8}$$

where L is the distance between perforations, d is the film thickness, and N is the number of droplets into which each filament breaks up. The diameter of the droplets, for a uniform nanowire filament, is determined by the Rayleigh instability criterion[29] and is expected to be ~ 3.78 times the radius of the filament r. So the number of drops will be dependent on the film thickness. As the length of the filament will be proportional to L, we get

$$\text{Volume of filament } V_f \propto L\pi r^2 \propto L^2 d, \quad \text{so } R \propto \sqrt{Ld}. \tag{9}$$

From the results shown in Fig. 1(e) and from analysis of the data from the ELN of the other metals, it can be seen that, rather than R varying with $\sqrt{d}$, R increases superlinearly with d indicating that L must be increasing very rapidly with increasing d. This is exactly what would be predicted if we are relying on thickness fluctuations to provide the perforations. A thickness fluctuation will have to be larger (i.e., more standard deviations from the mean, occurring less frequently, and being more widely spaced) for a 15 nm thick film to have the same effect when compared to a 5 nm thick film.

Once the film has broken up into isolated droplets, any subsequent pulses will remelt the droplets (or just the surfaces of the larger drops). Although the ELN has been performed in a scanning mode, with multiple laser spots on each area, experiments show that only a single laser shot at the highest energy is required to nanostructure the films. Unless the droplets are mobile on the surface no further modification is expected unless the fluence is high enough to boil off the surface material, as is observed with the Au films at fluences higher than the threshold. Careful examination of the images in Figs. 3(b) and 3(c) shows that the size of the larger droplets appears to have increased at the higher fluence. This is also observed for Ag in Figs. 3(f) and 3(g). This is likely a consequence of some of the droplets being mobile on the surface, as their surface boils, allowing some of the surviving drops to coalesce. This phenomenon was not observed for Ni and Ti thin films, where the boiling point was not reached. In fact by masking areas of the film and only depositing metal through the mask we can demonstrate that the droplets in general are not mobile unless they boil. Figure 10 shows a SEM image of an array of patches of Ni droplets produced by ELN of a patterned Ni film. Lithographic and masking techniques can be used in conjunction with ELN with little spread of the metal out of the defined areas. This will be important if ELN is to be used in conjunction with traditional device fabrication techniques. At extremely high laser fluences we enter the ablation regime, where the thin film melts and splits into droplets, which can then boil. However, as they boil these droplets appear to fragment into smaller nanoparticles (<10 nm in diameter), which can be left on the substrate

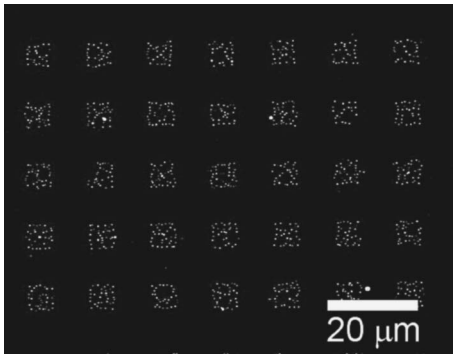

FIG. 10. SEM image of an array of patches of Ni droplets produced by ELN of a patterned Ni film. Lithographic and masking techniques can be used in conjunction with ELN with little spread of the metal out of the defined areas.

We should also consider the temperature rise of the substrate during the process. For a 4 cm^2 Si substrate, 1 mm thick, irradiated by one laser pulse at 500 mJ the expected final temperature rise is calculated as ~ 0.15 K, ignoring heat conduction into the surroundings. Thus, unless a very large number of shots per unit length is used during the scan, the substrate should remain at a low macroscopic temperature. In comparison, the production of Ni nanoislands by thermal annealing of thin Ni films, for example, typically requires the whole substrate to be raised to high temperatures ($\sim$800–900 K) for extended periods of time. The ELN technique also differs from thermal annealing as the islands are formed by bulk instabilities in a molten thin film, rather than by a process analogous to Ostwald ripening where mass transport

of individual metal atoms or clusters occurs at temperatures below the melting point of the metal. ELN offers a method for fabricating nanostructured metal-on-oxide substrates, rapidly, over a large area and at low macroscopic temperatures.

IV. CONCLUSION

The underlying physical mechanisms of the ELN technique were investigated, for a carefully chosen selection of metals with differing physical and thermodynamic properties, and differing propensities for oxide formation. A finite element model was introduced that can be used to model the melting of very thin metal-on-oxide films by pulsed lasers. Using the results from ELN experiments and simulations using this model, the thermal conductivity of the substrate was shown to be a controlling parameter on the laser fluence required to melt very thin films. Once molten, it is suggested that the breakup of the film into nanodroplets only occurs when the liquid metal does not wet the substrate, the heat of formation of the metal oxide being a critical parameter. The effect of film thickness fluctuations on the local threshold for melting is then suggested as the main influence on the nanoparticle size. ELN is expected to be suitable for producing nanoparticles of a large range of different materials, where poor wetting of substrate by the liquid phase is observed.

ACKNOWLEDGMENTS

The authors would like to thank the EPSRC Portfolio Grant and the Carbon Based Electronics Programme for funding the project.

*Electronic address: s.henley@eim.surrey.ac.uk

[1] G. J. Galvin, M. O. Thompson, J. W. Mayer, R. B. Hammond, N. Paulter, and P. S. Peercy, Phys. Rev. Lett. **48**, 33 (1982).
[2] D. S. Ivanov and L. V. Zhigilei, Phys. Rev. B **68**, 064114 (2003).
[3] H. Kisdarjonoa, A. T. Voutsas, and R. Solanki, J. Appl. Phys. **94**, 4374 (2003).
[4] P. Baeri, S. U. Campisano, G. Foti, and E. Rimini, J. Appl. Phys. **50**, 788 (1979).
[5] V. Y. Balandin, R. Niedrig, and O. Bostanjoglo, J. Appl. Phys. **77**, 135 (1995).
[6] J. D. Carey, L. L. Ong, and S. R. P. Silva, Nanotechnology **14**, 1223 (2003).
[7] U. Diebold, J. M. Pan, and T. E. Madey, Phys. Rev. B **47**, 3868 (1993).
[8] F. C. Frank and J. H. Van der Merwe, Proc. R. Soc. London, Ser. A **198**, 205 (1949).
[9] M. Volmer and A. Weber, Z. Phys. Chem. (Leipzig) **119**, 277 (1926).
[10] I. N. Stranski and L. Krastanow, Akad. Wiss. Lit. Mainz Abh. Math. Naturwiss. Kl. **146**, 797 (1937).
[11] M. Chhowalla, K. B. K. Teo, C. Ducati, N. L. Rupesinghe, G. A. J. Amaratunga, A. C. Ferrari, D. Roy, J. Robertson, and W. I. M. Milne, J. Appl. Phys. **90**, 5308 (2001).
[12] T. Goodson, O. Varnavski, and Y. Wang, Int. Rev. Phys. Chem. **23**, 109 (2004).
[13] H. Kodama, S. Monose, N. Ihara, T. Uzumaki, and A. Tanaka, Appl. Phys. Lett. **83**, 5253 (2003).
[14] P. Colomban, J. Mater. Res. **13**, 803 (1998).
[15] S. Iijima, Nature (London) **354**, 56 (1991).
[16] S. J. Henley, C. H. P. Poa, A. A. D. T. Adikaari, C. E. Giusca, J. D. Carey, and S. R. P. Silva, Appl. Phys. Lett. **84**, 4035 (2004).
[17] A. M. Morales and C. M. Lieber, Science **279**, 208 (1998).
[18] Y. Hau, H. Kondoh, T. Ohta, and S. Gao, Appl. Surf. Sci. **241**, 218 (2005).
[19] G. Compagnini, A. A. Scalisi, and O. Puglisi, J. Appl. Phys. **943**, 7874 (2003).
[20] L. Castaldi, K. Giannakopoulos, A. Travlos, and N. D, Appl. Phys. Lett. **85**, 2854 (2004).
[21] R. H. Magruder, L. Yang, R. F. Haglund, C. W. White, L. Yang, R. Dorsinville, and R. R. Alfonso, Appl. Phys. Lett. **62**, 1730 (1993).
[22] M. N. R. Ashfold, F. Claessyens, G. Fuge, and S. J. Henley, Chem. Soc. Rev. **33**, 23 (2004).
[23] B. Toftmann, J. Schou, and J. G. Lunney, Phys. Rev. B **67**, 104101 (2003).
[24] R. E. Leuchtner, D. B. Chrisey, J. S. Horwitz, and K. S. Grabowski, Surf. Coat. Technol. **51**, 476 (1992).
[25] R. Dolbec, E. Irissou, M. Chaker, D. Guay, F. Rosei, and M. A. E. Khakani, Phys. Rev. B **70**, 201406(R) (2004).
[26] Scion Image, www.scioncorp.com
[27] N. Eustathopolous and B. Drevet, Mater. Sci. Eng., A **249**, 176 (1998).
[28] R. Sangiorgi, M. L. Muolo, D. Chatain, and N. Eustathopolous, J. Am. Ceram. Soc. **71**, 742 (1988).
[29] L. Rayleigh, Proc. London Math. Soc. **10**, 4 (1879).
[30] M. E. Toimil Molares, A. G. Balogh, T. W. Cornelius, R. Neumann, and C. Trautmann, Appl. Phys. Lett. **85**, 5337 (2004).
[31] WebElements, www.webelements.com
[32] J. Hodak, I. Martini, and G. V. Hartland, Chem. Phys. Lett. **284**, 135 (1998).
[33] T. Ohashi, K. Kuroda, and H. Saka, Philos. Mag. B **65**, 1041 (1992).
[34] *Handbook of Optical Constants of Solids*, edited by E. D. Palik (Academic Press, Orlando, 1984).
[35] V. E. Henrich and P. A. Cox, *The Surface Science of Metal Oxides* (Cambridge University Press, Cambridge, 1994).